Combustion and Flame 223 (2021) 77–87

Contents lists available at ScienceDirect

Combustion and Flame

journal homepage: www.elsevier.com/locate/combustflame

Experimental and kinetic study on the low temperature oxidation and pyrolysis of formic acid in a jet-stirred reactor

Geyuan Yin, Jiawei Xu, Erjiang Hu*, Qunfei Gao, Haochen Zhan, Zuohua Huang

State key Laboratory of Muliphase Flow in Power Engineering, Xi'an Jiaotong University, Xi'an, People's Republic of China

ARTICLE INFO

Article history:
Received 24 June 2020
Revised 30 September 2020
Accepted 1 October 2020

Keywords:
Formic acid
Low temperature oxidation
Pyrolysis
Rate coefficient calculation
Chemical kinetic model

ABSTRACT

A comprehensive experimental and kinetic study on the low temperature oxidation and pyrolysis of formic acid was conducted. Species profiles measurements were performed in a jet-stirred reactor (JSR) at the temperature range of 600–1100 K under atmospheric pressure, with a fixed residence time of 2.0 s and for the equivalence ratios ranging from 0.5 to ∞ (pyrolysis). High-level quantum calculation was used to obtain the accurate rate coefficients of missing reactions in Glarborg model. A detailed kinetic mechanism, derived from Glarborg model, has been developed based on high-level quantum calculation and validated with the species profiles obtained in this work and laminar flame speeds presented in our group. Reaction pathway and sensitivity analysis were investigated to get the deep insight of the oxidation of formic acid via the modified model. The results showed that unimolecular fuel decomposition reactions dominated the pyrolysis process while H abstraction reactions with the further consumption of the radicals are more important in the oxidation of formic acid. In addition, H abstraction reactions via HO2 become important at relatively low temperature.

1. Introduction

It is currently accepted that carboxylic acids would enhance the acidity of the atmosphere as well as sulphuric and nitric acids and then leads to acid rain [1,2]. The production of carboxylic acids in atmosphere is from the biomass pyrolysis or the combustion in the engine. The secondary production from alkenes or the direct exhaust emissions form engine is involved in the formation of carboxylic acids. In another way, carboxylic acids are important components of bio-oil [3] whose reforming has gained more and more attention with the potential to be clean-burning fuel. In carboxylic acids, formic acid (HOCHO) is the simplest one and is one of the most important acids of emitted hydrocarbons.

In addition, hydrogen is widely regarded as an alternative fuel. However, it is not a liquid and demands significant investments in tanks for storage. With this problem, there is big interest in hydrogen containing molecules, called "hydrogen carrier". Formic acid has been regarded as a hydrogen carrier [4]. It undergoes a simple reaction process, HOCHO<=>CO_2 + H_2, to produce hydrogen. It is of high potential as an e-fuel in internal combustion engine. Therefore, in order to investigate the reductions of this pollutant and the potential in combustion, it is of great importance to investigate the pathways involved in its consumption.

Theoretical kinetic study of HOCHO has been investigated through high-level quantum calculation. Chang et al. [5] conducted the calculation of unimolecular decomposition reactions of HOCHO using G3M(CC1) method combined with microcanonical RRKM theory. The calculated rate coefficients agree well with the available experimental data at high temperature. Anglada [6] investigated the potential energy surface (PES) of abstraction and addition reactions between HOCHO and hydroxyl radical. Besides, the PES of HOCO with HO_2 and O_2 were obtained by Yu et al. [7,8].

Chemical kinetic study on HOCHO has also been examined in flow reactor by Blake et al. [9]. Golden et al. measured the rate coefficients of HOCO decomposition reactions producing CO+OH in a shock tube [10]. Gaydon and Wolfhard performed a spectroscopic study of low-pressure HOCHO/O_2 premixed flame experiments to investigate the oxidation kinetic of HOCHO [11]. The major intermediates are CO and OH while C_2, HCO and CH radicals were not detected. Marshall and Glarborg [12] presented a detailed chemical kinetic model of HOCHO based on high-level quantum calculation and validated the laminar flame speeds measured by de Wilde and van Tiggelen [13] via Bunsen burner in 1968. In our previous work [14], laminar flame speeds of formic acid were measured at equivalence ratios of 0.4–1.6, initial temperatures of 423–453 K and atmospheric pressures in a constant volume combustion

* Corresponding author.
E-mail address: hujiang@mail.xjtu.edu.cn (E. Hu).

https://doi.org/10.1016/j.combustflame.2020.10.005
0010-2180/

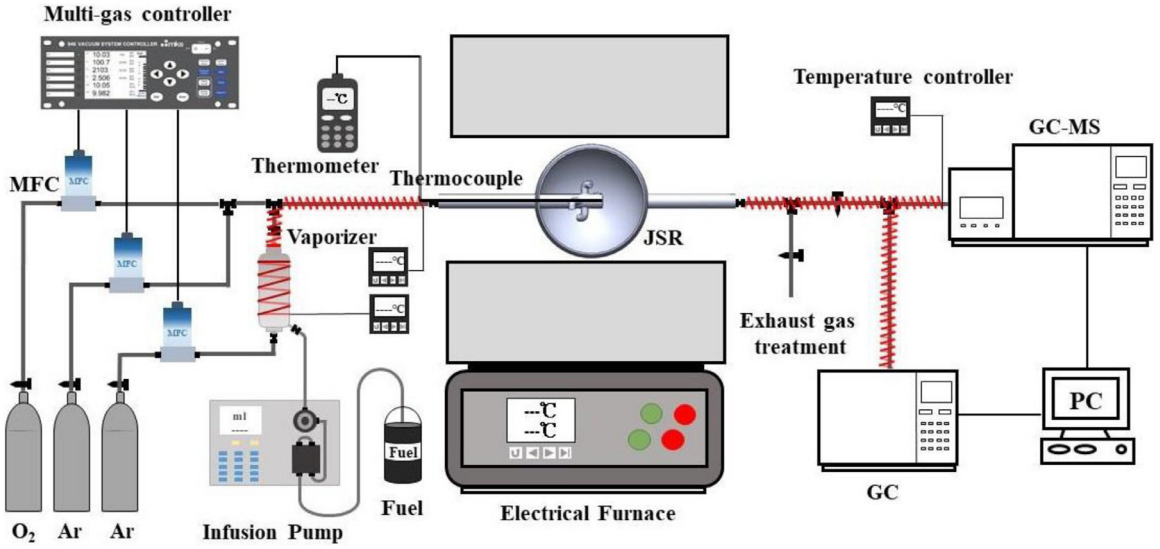

Fig. 1. The schematic diagram of JSR.

bomb. Chemical kinetic models (Glarborg model and AramcoMech 3.0 [15]) were validated against the measured experimental data.

Therefore, despite the interest in formic acid as pollutant from combustion and hydrogen carrier material, researches on its gas-phase chemistry is still scarce. The objective of this work is to provide a wider experimental database of formic acid. Low temperature oxidation and pyrolysis in JSR were conducted at the temperature range of 600–1100 K under atmospheric pressure, with a fixed residence time of 2.0 s and for the equivalence ratios ranging from 0.5 to ∞ (pyrolysis). The other one is to modify Glarborg model based on ab initio calculations for key elementary reactions under current conditions, together with the high-level calculated thermodynamic data. The model containing low-to-high temperature oxidation reactions was validated with mole fractions in JSR and laminar flame speeds. Finally, detailed kinetic analysis was performed to provide deeper insight into the potential reductions and reformation to obtain hydrogen of formic acid.

2. Experimental method

This experimental setup has been validated with the experimental data in literatures and details are shown in our previous work [16,17]. The schematic diagram is shown in Fig. 1. It can be divided into four parts, reacting system, fuel supply system, heating system and detection system. The reactor is a laboratory-scale spherical fused silica JSR with the volume of 87 cm^3. Jet stirred reactor is a typical zero-dimensional reactor. The main principle of JSR is to power high-speed jet of gaseous and makes them homogeneous mixed. Computational fluid dynamics (CFD) is used to simulate the homogeneity in the reactor and the result is shown in Fig. S1. Firstly, the tracer gas (CO_2) was injected into JSR and then it was diluted by N_2. Figure S1 in Supplemental data 1 presents the concentration of CO_2 in JSR changing with time. It can be seen that at any time the distribution of CO_2 is uniform. Besides, the concentration of CO_2 decreases with the increase of N_2.

Formic acid (Aladdin Co. Ltd., of 99% purity) was evaporated in a chamber at 393 K, which is 20 K higher than the boiling point. The flow rates of oxygen and helium of 99.995% purity were controlled by MKS mass-flow controllers separately. Residence time was maintained as 2 s via changing the flow rate of mixtures with temperature, while the mole fraction of formic acid is 2% with oxygen at the equivalence ratios of 0.5, 1.0, 2.0 and diluted in helium. The uncertainty of flow rate measurements is about 0.5% leading to maximum uncertainty of around 2% in residence time. For heating system, the reactant and product mixtures were preheated to 393 K to avoid condensation, while a furnace (SK-G05123K, ZH) can provide a 440 mm heating zone with a stable target temperature for JSR. Therefore, the reactant mixtures were heated to target temperature before into the reactor to eliminate temperature gradient. Moreover, a K-type thermocouple was set inside the center of JSR to obtain the actual reaction temperature. As to detection system, the outlets were analyzed online by GC–MS (Agilent 7890B-5977A) and GC (Agilent 7890B) using flame ionization detector (FID) and thermal conductivity detector (TCD). Those were used to quantify HOCHO, CO_2, CO, H_2 and O_2. The limit of detection for species was 1 ppm using FID, while it was 10 ppm for species analyzed using TCD. The relative uncertainty in the mole fraction of species was estimated as $\pm$ 10%. Besides, carbon balance was checked for every sample and found to be good within $<$ 5%. Pretty good experimental repeatability and reproducibility can be obtained through multiple measurements at least three times. Multiple measured mole fractions of O_2 are shown in Fig. S2 in Supplemental data 1. Good experimental repeatability and reproducibility can be found. Besides, the mole fractions of O_2 in each time are listed in Supplemental data 3 with the discrepancies between the measured data under same conditions. The discrepancies of the data under same conditions are less than 2%.

3. Theoretical method

Some important elementary reactions of HOCHO at low temperature have not been previously characterized theoretically. In this work, high-level quantum calculations for them were conducted to get accurate rate coefficients. The potential energy surfaces (PESs) are obtained using compound methods. Firstly, structures are optimized and frequencies are calculated using M06–2X [18] functional with 6–311++G(d,p) basis set scaled by a factor of 0.946 [19]. Then, single point energy calculation is performed via couple cluster theory with explicit correlations, CCSD(T)-F12 [20] with cc-pVTZ-F12 and cc-pVQZ-F12 basis sets. For all first-order saddle points, the imaginary mode is visually inspected, and intrinsic reaction coordinate (IRC) calculations confirmed that the correct saddle points are obtained. As to barrierless reaction pathways, single reference method does not work, while multireference theory is adopted. CASPT2/cc-pVTZ [21] is used to optimize the struc-

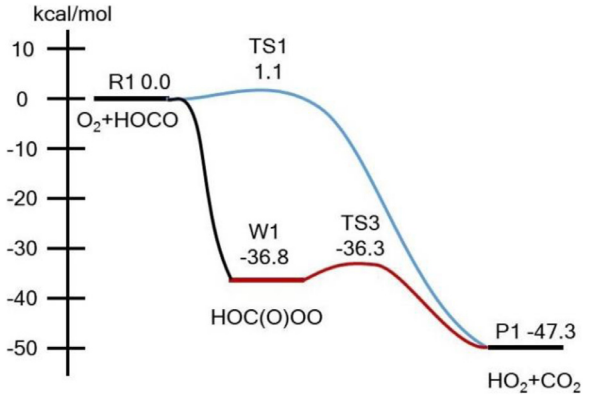

Fig. 2. Potential energy surface of HOCO with O_2 at CCSD(T)-F12/CBS//M06-2X/6–311++G(d,p) level. (For interpretation of the references to color in this figure, the reader is referred to the web version of this article.)

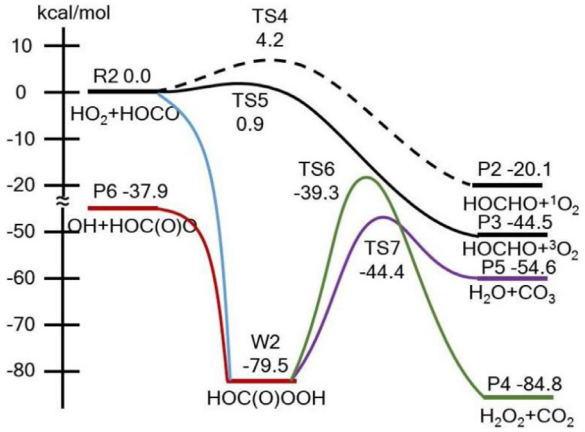

Fig. 3. Potential energy surface for HOCO with HO_2.

ture, while CASPT2/CBS(T + Q) is adopted for high-level energy calculation. The choice of active space is based on case-by-case, described below. The complete basis set limit was extrapolated from the triple and quadruple zeta basis set calculations assuming an inverse power law [22]:

$$E_{CBS} = E_{QZ} + (E_{QZ} - E_{TZ})\frac{4^4}{5^4 - 4^4} \quad (1)$$

The pressure- and temperature-dependent rate coefficients are calculated using the RRKM/ME code in Mess [23,24]. Rigid-rotor-harmonic-oscillator model (RRHO) is adopted to calculate the partition function of transition states, reactants and products. Low-frequency torsional modes are treated as 1-D or 2-D internal rotors with the rotational potentials estimated by a relax scan at M06–2X/6–311++G(d,p) level.

Both the HO2 and O2 added to HOCO radicals are barrierless reactions. Harmonic transition state theory failed to obtain accurate rate coefficients. Instead, variable reaction coordinate transition state theory (VRC-TST) [25] is used to calculate the E, J resolved microcanonical rate coefficients. All DFT calculations were done in Gaussian [23,26,27] and others were performed in MOLPRO [28].

4. Chemical kinetic model

The chemical kinetic model of formic acid was developed based on the mechanism presented by Marshall and Glarborg [12]. The Glarborg model consists of 34 species and 84 reactions. In this work, missed reaction classes were added according to high-level quantum calculation and some were modified according to the JSR data in this work, including HOCO radicals with O_2 and HO_2, OH addition reaction and further decomposition reactions, H abstraction reactions with H and HO_2, fuel unimolecular decomposition reactions. The single-point energies, zero-point corrections, and T1 diagnostics [29] are listed in Table S1 to Table S3 in the Supplemental data 1.

HOCO with O_2: This reaction class plays an important role in the oxidation of HOCHO at low to intermediate temperature. The calculated potential energy surface was presented in Fig. 2. The main disproportionation reaction, which is the blue line shown, proceeds TS1 and leads to HO_2 and CO_2. Besides, O_2 can add to radical center leading to HOC(O)OO, through a barrierless way. The active space is 11 electrons in 8 orbitals, (11e, 8o), consisting of the π and π^* in O_2, π and π^* in C = O and the carbon-centered radical orbital. The bimolecular product channel with low barrier heights is bond-fission reaction forming the same products as TS1. In addition, it would be possible for thermally actived reactants to form HO_2 and CO_2 directly, skipping the well HOC(O)OO. Glarborg model only contains this bimolecular product channel but omitted O_2 addition reaction and H abstraction reaction. Thus, these two reactions have been calculated and added into the modified model.

HOCO with HO_2: This reaction class is always promoting one at low to intermediate temperatures. The PES of HOCO with HO_2 obtained at CCSD(T)-F12/CBS//M06–2X/6–311++G(d,p) are presented in Fig. 3. There are two H abstraction reactions as the black line shown. H transfer between HOCO with HO_2 on the singlet potential energy surface as dashed line shown through TS4 leads to HOCHO and $^1O_2$. This reaction has little effect on the overall rate coefficients with relatively higher barrier height. HOCO can also abstract H from HO_2 on the triplet PES via TS5, leading to HOCHO and $^3O_2$. The T1 diagnostic of $^3O_2$ is just slightly higher than 0.03. Single reference method can be used to obtain reasonable rate coefficients of H abstraction reactions of triplet oxygen and alkene as presented in Zhou et al. [30] In addition, HO_2 can add to radical center, the minimum active space is four electrons in four orbitals, (4e, 4o), which accounts for the three orbitals needed to describe the delocalized π-system in allylic compounds, plus one orbital for the oxygen-centered radical on HO_2. This barrierless reaction produces HOC(O)OOH. The energized HOC(O)OOH adduct is either stablilized via collision or decomposes to HOC(O)O and OH through a barrierless way. The active space is set to 6 electrons in 4 orbitals, consisting of the π and π^* in O_2. HOC(O)OOH can also be consumed by water elimination to form H_2O and CO_3 and H_2O_2 and CO_2. In addition, similar to HOCO + O_2, thermally actived reactants directly form HOC(O)O + OH, H_2O + CO_3 and H_2O_2 + CO_2. However, in Glarborg model, it only contains H abstraction reaction HOCO + HO_2<=>HOCHO + O_2. The dominant barrierless channel with the further bimolecular product channels at intermediate temperature is missed. Therefore, rate coefficients of the others have been calculated and added into the modified model.

The calculated total rate coefficient of HOCO+HO_2 is compared with allyl + HO_2 obtained by Goldsmith et al. [31] as shown in Fig. 4. They are in close agreement with maximum discrepancies of a factor of 2.

HOCHO with OH: OH addition reactions are missed in Glarborg model which plays a significant role in low temperature oxidation. Thus, we have conducted ab initio calculations for OH added to C = O bond. Figure 5 shows the potential energy diagram for HOCHO with OH. Reactant proceeds via reversible addition across the C = O group, with barrier height of 5.38 kcal/mol, yielding $HCO(OH)_2$. $HCO(OH)_2$ further isomerizes to $C(OH)_3$ and both radicals decompose to $CO(OH)_2$ + H. All of the above reactions are added into the modified model.

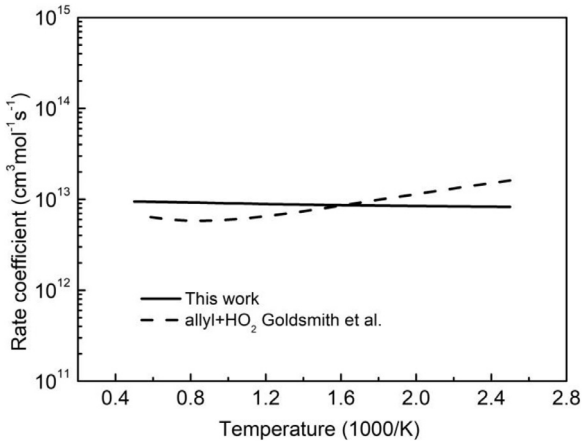

Fig. 4. Total rate coefficient of HO_2+HOCO obtained in this work compared with previous theoretical data.

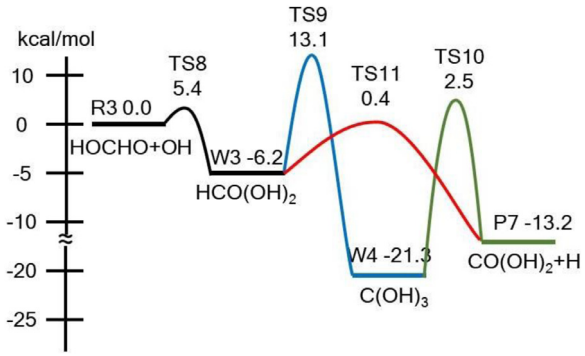

Fig. 5. Potential energy diagram for HOCHO with OH.

H abstraction reactions: Rate coefficients of H abstract from carbon: H+HOCHO<=>HOCO + H_2 is increased by a factor of 2 to match the mole fraction of H_2 in JSR, which is within the uncertainty of the calculation. H abstraction reactions by HO_2 should be important in low to intermediate temperature range. However, this reaction class shows no contribution in 900 K for fuel consumption using Glarborg model. Rate coefficients of HO_2+HOCHO<=>HOCO + H_2O_2 obtained in this work is compared with HO_2+CH_3OH<=>CH_2OH + H_2O_2 calculated by Klippenstein et al. [32] and HO_2+HOCHO<=>HOCO + H_2O_2 published in Marshall and Glarborg. The result is shown in Fig. 6. The discrepancy is about 6 orders of magnitude at 600 K with Glarborg model as the red dot line shown. Therefore, reaction HO_2+HOCHO<=>HOCO + H_2O_2 has been reconsidered via ab initio calculation and was multiplied by a factor of 2 to predict well formic acid consumption in JSR data. The overall agreement between the current work and results by Klippenstein et al. [32] is quite good at both high and low temperatures with maximum discrepancies of a factor of 2–3.

The uncertainty of rate coefficients calculated by Marshall and Glarborg is not provided which arises partially from uncertainties in the predicted barrier height (around 1.0 kcal/mol). [32] Thus, the barrier heights alter by ± 1.0 kcal/mol as shown in Figs. S3 and S4. With the decrease of barrier height by 1.0 kcal/mol, the rate coefficient increased by a factor from 1.5 to 3.5 at the temperature of 1600 K to 400 K. In addition, in similar system, the abstraction reaction of CH_3OH by HO_2 [32], the best estimate of the uncertainty factor is between 1.5 and 2.5 over the key 600–2000 K range. Thus, in this work, we increase the rate coefficient by a factor of 2 to match the mole fraction of H_2 in JSR.

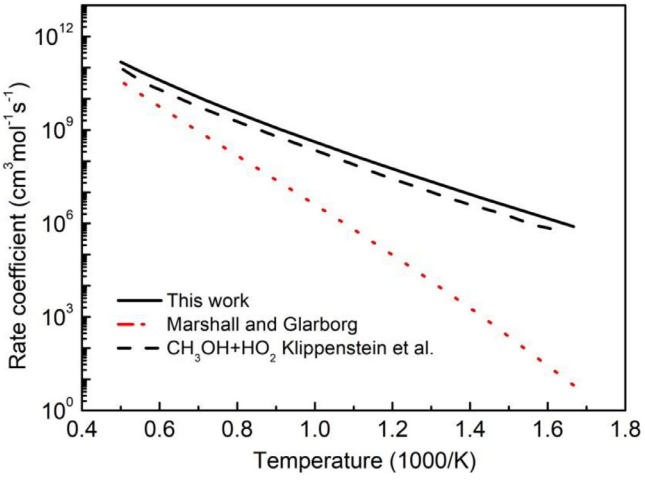

Fig. 6. Rate coefficient of HO_2+HOCHO<=>HOCO + H_2O_2 obtained in this work compared with previous theoretical data. (For interpretation of the references to color in this figure, the reader is referred to the web version of this article.)

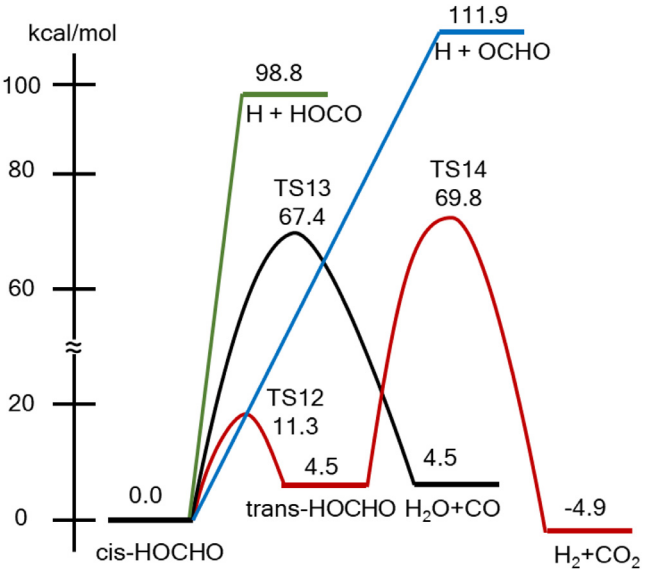

Fig. 7. Potential energy surface for unimolecular decomposition of HOCHO.

Unimolecular decomposition reactions: Figure 7 presents the PES of unimolecular decomposition of HOCHO. It is obviously that two important reactions which should be highlighted are HOCHO<=>CO+H_2O, HOCHO<=>CO_2+H_2 with relatively lower barrier height. The C–H bond fission reaction channels have about 30 kcal/mol higher barrier heights. Thus, CO+H_2O and CO_2+H_2 are largely produced through pyrolysis of HOCHO. The absence of radical producing dissociation channels has also been confirmed by Glarborg and Klatt et al. [12,33]. Nevertheless, as the experimental and simulated mole fractions of CO_2 and H_2 shown in Fig. 8, the current branching ratio of HOCHO<=>CO_2+H_2 is too small at low temperature but too big at high temperature. The low temperature rate coefficient is obtained from Blake et al. [9] measured in flow reactor at the temperature range of 380 to 1000 K with the high temperature rate almost unchanged from the Glarborg model.

The unimolecular decomposition reactions of HOCHO have been well investigated both experimentally and theoretically. The rate coefficient of HOCHO<=>CO_2 + H_2 in this work is compared with the theoretical result from Chang et al. which matches well with the calculated result and experimental data in literatures at the temperature range of 1000–2000 K. As shown in Fig. 9(a). In

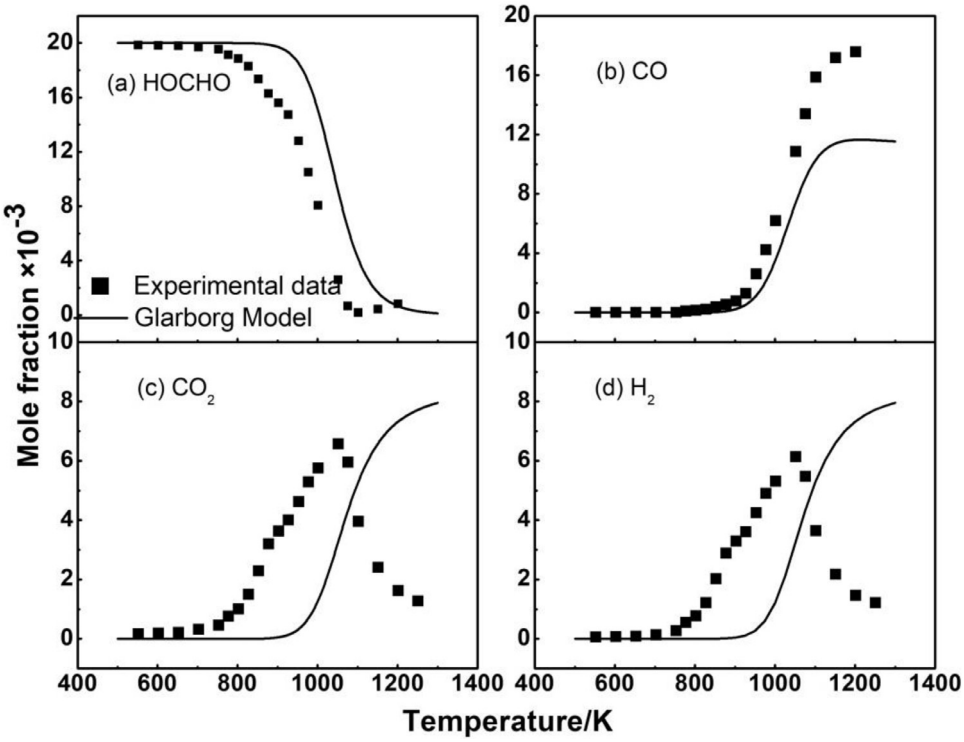

Fig. 8. Mole fractions in the pyrolysis of HOCHO at the pressure of in 1 atm and with the residence time of 2 s.

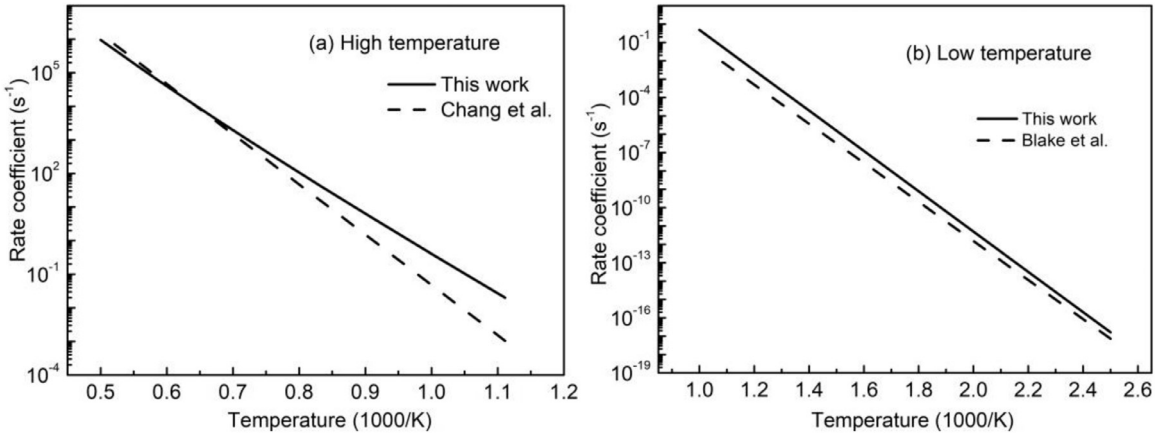

Fig. 9. Rate coefficient of HOCHO<=>CO_2 + H_2 obtained in this work compared with previous data.

addition, rate coefficient of HOCHO<=>CO_2 + H_2 in this work agrees well with Chang et al. [5] at relatively high temperature. In addition, we also compared the rate coefficient in this work with the experimental data measured in flow reactor by Blake et al. [9] at the temperature of 380–1000 K. Good agreement can also be observed.

The key reactions calculated or modified above with rate coefficients are listed in Table 1.

Thermochemistry: Thermochemical data of the species in a kinetic model are essential to estimate the reverse rate of the reactions and species properties such as enthalpy, entropy, heat capacity. In this work, the thermochemistry of newly added species has been calculated via high-level quantum calculation. Frequencies at M06-2X/6–311++G(d,p) level scaled by a factor of 0.946 are used to obtain enthalpy, entropy and heat capacity. The combination of G4, G3 and CBS-APNO are adopted for the enthalpy of formation as shown in Table 2. Mechanism in Chemkin format is shown in Supplemental data 2.

5. Model validation

5.1. Speciation validations

The pyrolysis of formic acid has also been experimentally studied in JSR at the temperature range of 600–1400 K, which can provide information only for the thermal dissociation of HOCHO. Although these reactions seem well established in high temperature, they give unreasonable prediction of the produced species in low to intermediate temperature range, especially for CO_2 and H_2, which means HOCHO<=> CO_2+H_2 should be revised. After the modification, the profiles of H_2, CO_2 and CO can be well predicted as shown in Fig. 10.

Table 1
Reaction subset for formic acid oxidation. Parameters in Arrhenius expression $k=AT^n\exp(-E/RT)$. Unites are mol, cm, s, K.

Num.	Reaction	A	n	E_a	Source
1	HOCHO<=>CO+H_2O	7.5E+14	0.0	68,710	Mod.
2	HOCHO<=>CO_2+H_2	1.42E-07	5.33	43,479	Mod.
3	HOCHO+OH<=>HOCO+H_2O	2.70E-01	3.93	12,500	Cal.
4	HOCHO+HO_2<=>OCHO+H_2O_2	3.7E+01	2.98	25,348	Cal.
5	HOCHO+H<=>HOCO+H_2	4.3E+02	3.272	4858	Mod.
6	HOCO+O_2<=>HOC(O)OO	8.71E+00	2.17	−2871.0	Cal.
	PLOG/1.000E-02 4.49E-09 0.00-17910.0/				
	PLOG/1.000E-01 3.68E-06 0.00-10760.0/				
	PLOG/1.000E+00 2.51E-11 0.00-24300.0/				
	PLOG/1.000E+01 4.70E-12 5.21 4355.0/				
	PLOG/1.000E+02 8.71E+00 2.17-2871.0/				
7	HOC(O)OO<=>CO_2+HO_2	3.22E+12	−0.33	5655.0	Cal.
	PLOG/1.000E-02 8.16E+07 0.00 2680.0/				
	PLOG/1.000E-01 3.42E+08 0.11 3091.0/				
	PLOG/1.000E+00 6.35E+10-0.31 4084.0/				
	PLOG/1.000E+01 1.04E+12-0.40 4916.0/				
	PLOG/1.000E+02 3.22E+12-0.33 5655.0/				
8	HOCO+O_2<=>CO_2+HO_2	1.79E+16	−1.23	909.6	Cal.
9	HOCO+HO_2<=>HOCOO+OH	7.28E+12	0.02	118.6	Cal.
10	HOCO+HO_2<=>H_2O+CO_3	9.23E+08	0.68	−549.0	Cal.
11	HOCO+HO_2<=>H_2O_2+CO_2	3.31E+11	0.16	−196.5	Cal.
12	HOCO+HO_2<=>HOC(O)OOH	1.11E+32	−6.34	5754.0	Cal.
	PLOG/1.000E-02 2.63E+96-27.42 55100.0/				
	PLOG/1.000E-01 3.81E+15-3.25 15410.0/				
	PLOG/1.000E+00 3.31E+18 -3.72 6721.0/				
	PLOG/1.000E+01 1.59E+28-5.94 4270.0/				
	PLOG/1.000E+02 1.11E+32-6.34 5754.0/				
13	HOC(O)OOH<=>HOCOO+OH	1.29E+32	−5.22	59410.0	Cal.
	PLOG/1.000E-02 1.23E+46-10.57 60710.0/				
	PLOG/1.000E-01 2.29E+48-10.80 62760.0/				
	PLOG/1.000E+00 1.84E+46-9.84 63380.0/				
	PLOG/1.000E+01 1.69E+40-7.79 62080.0/				
	PLOG/1.000E+02 1.29E+32-5.22 59410.0/				
14	HOCHO+OH<=> $HCO(OH)_2$	1.78E+17	−2.50	1980.0	Cal.
	PLOG/1.000E-02 3.46E+00 0.00 0.0/				
	PLOG/1.000E-01 1.19E+05 0.00 4474.0/				
	PLOG/1.000E+00 1.99E+04 0.56 1352.0/				
	PLOG/1.000E+01 8.04E+10-1.11 564.0/				
	PLOG/1.000E+02 1.78E+17-2.50 1980.0/				
15	HOCHO+OH<=>H+$HCO(OH)_2$	7.46E+07	1.36	1421.0	Cal.
16	$HCO(OH)_2$<=>H+$CO(OH)_2$	3.77E+15	−1.22	7245.0	Cal.
	PLOG/1.000E-02 2.73E+06 0.00 0.0/				
	PLOG/1.000E-01 7.38E+08 0.00 3300.0/				
	PLOG/1.000E+00 7.27E+11-0.65 4610.0/				
	PLOG/1.000E+01 3.11E+14-1.17 6039.0/				
	PLOG/1.000E+02 3.77E+15-1.22 7245.0/				

Table 2
Thermodynamic properties of newly added species in the mechanism. Units are kcal·mol^{-1} for enthalpy, and cal·mol^{-1}K^{-1} for *S* and *Cp*.

Species	$\Delta H_{f,298}$	S_{298}	Cp_{300}	Cp_{400}	Cp_{600}	Cp_{800}	Cp_{1000}	Cp_{1500}
HOCO	−42.7	58.7	10.4	11.7	13.8	15.1	16.1	17.6
HOC(O)OO	−79.2	77.3	17.5	20.1	23.9	26.1	27.4	28.8
$HCO(OH)_2$	−85.0	78.0	17.1	20.7	24.7	27.0	28.7	31.3
$C(OH)_3$	−99.8	84.4	18.4	22.2	25.6	27.2	28.4	30.4
HOC(O)OOH	−121.6	82.2	19.6	22.3	26.4	28.9	30.5	32.8
HOCOO	−86.8	68.0	14.2	16.1	19.1	20.9	22.0	23.4
CO_3	−40.0	62.1	11.1	12.9	15.3	16.7	17.6	18.7
$CO(OH)_2$	−145.2	71.2	15.7	18.0	21.7	24.1	25.9	28.2

In this work, the concentration profiles of stable species during the oxidation of formic acid in a jet-stirred reactor have been measured at the equivalence ratios of 0.5–2.0, over a temperature range of 600–1100 K and atmospheric pressure. All the experimental data are listed in Supplemental data 3. Comparison between experimental data and simulated results using Modified model and Glarborg model is presented in Figs. 11–13. The oxidation of HOCHO seems to be difficult. It starts to be consumed at around 750 K and be totally consumed at 1050 K. The major species during the oxidation process are CO, CO_2, H_2 and H_2O. Unfortunately, under current conditions, our GC cannot detect H_2O. CO and H_2 reach the peak at around 950 K. Overall, there is better agreement between the modified model and the experimental data under the wide conditions than Glarborg model especially for H_2 and CO.

5.2. Flux analyses

To better understand the pyrolysis of HOCHO, flux analyses was performed as shown in Fig. 14 using both Modified model and Glarborg model. It is obvious that HOCHO is only consumed through two unimolecular decomposition reactions, yielding CO and H_2O, CO_2 and H_2, respectively at the whole temperature range. Flux obtained using Modified model is consistent with the experimental data. At 900 K, more than 60% of HOCHO are consumed via unimolecular decomposition reactions forming CO_2 and H_2. At 1000 K, majority of the HOCHO are consumed to produce CO and H_2O while the mole fractions of CO_2 and H_2 decrease with temperature quickly. In contrast, flux analyses results calculated using Glarborg model are unreasonable that at 900 K, the chain branching ratio of HOCHO<=>CO + H_2O is much higher than HOCHO<=>CO_2 + H_2 which is different from the experimental data.

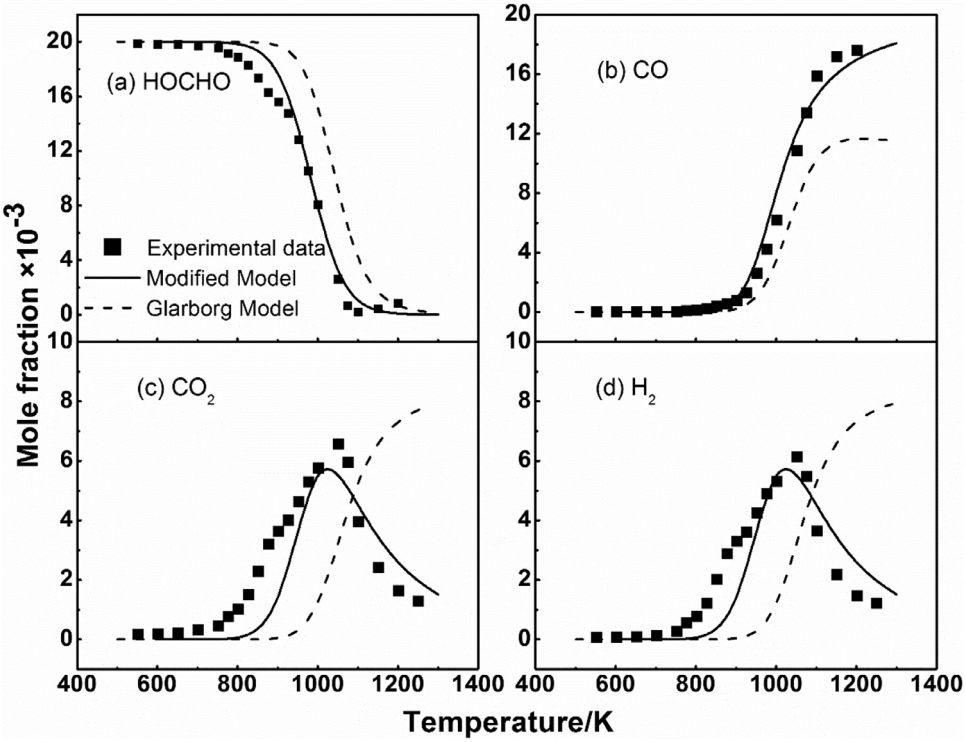

Fig. 10. Experimental and simulated mole fraction profiles of major species using Modified and Glarborg model in the pyrolysis of HOCHO in 1 atm and with the residence time of 2 s.

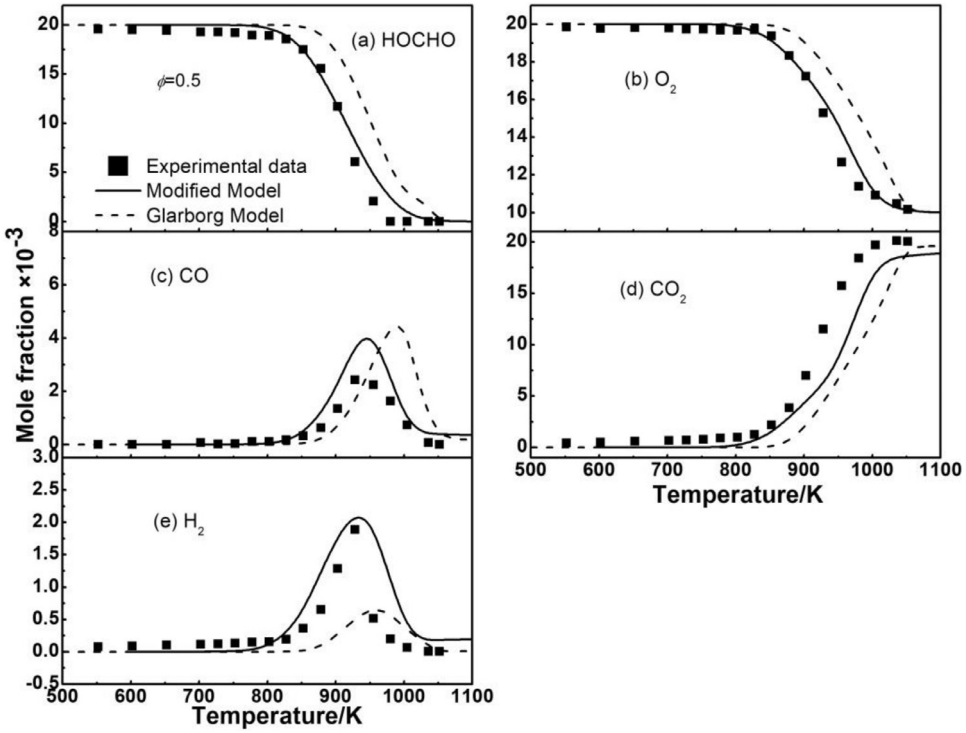

Fig. 11. Experimental and simulated mole fraction profiles of major species using Modified and Glarborg model in the oxidation of HOCHO at $\phi = 0.5$, in 1 atm and with the residence time of 2 s.

In order to provide the deep insight combustion kinetic of the formic acid oxidation which controls reactivity, the flux analyses was performed at 800 K, 900 K and 1000 K and $\phi = 1.0$ in Fig. 15.

At 800 K, the major pathway of fuel consumption is unimolecular decomposition reactions. The branching ratio of the bimolecular products $CO_2 + H_2$ is 48.1%. Formic acid is also consumed via H abstractions which is favored from C–H bond yielding H_2, H_2O, and H_2O_2 + HOCO, by H, OH and HO_2 radicals. accounting for 34.2%. OCHO radical is also produced via H abstraction reaction from O–H bond with much lower branching ration (4.7%). Under current condition, the reaction HOCO+O_2<=>CO_2 + HO_2 is the most dominant one for the consumption of HOCO with the branch-

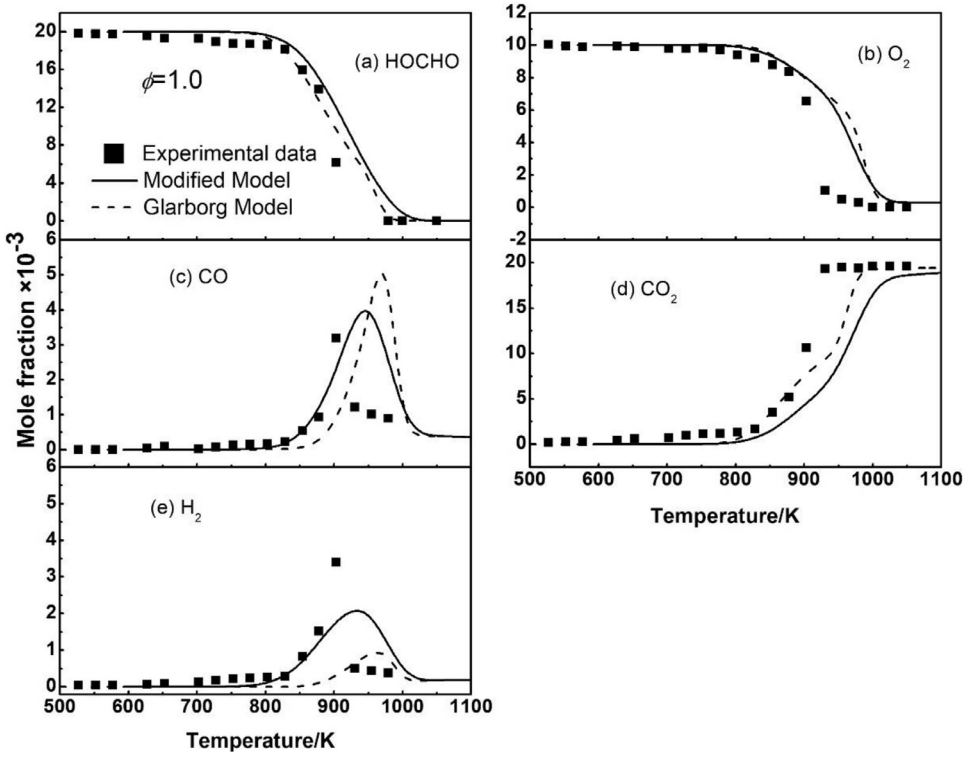

Fig. 12. Experimental and simulated mole fraction profiles of major species using Modified and Glarborg model in the oxidation of HOCHO at $\phi = 1.0$, in 1 atm and with the residence time of 2 s.

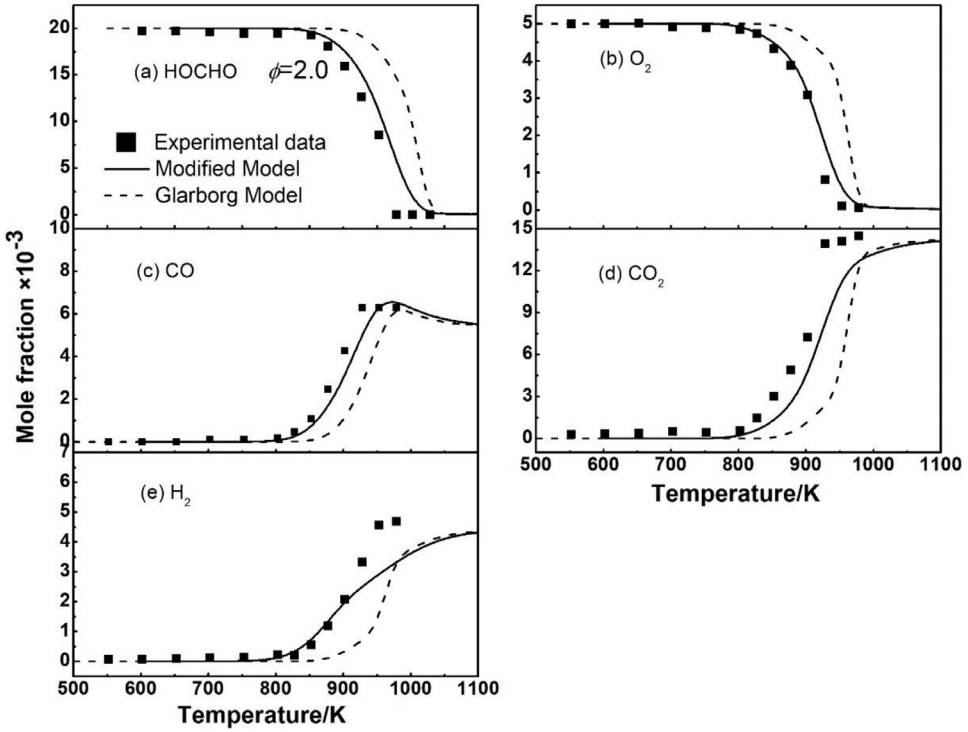

Fig. 13. Experimental and simulated mole fraction profiles of major species using Modified and Glarborg model in the oxidation of HOCHO at $\phi = 2.0$ in 1 atm and with the residence time of 2 s.

ing ratio of 90.1%. It has to be mentioned that OH addition reaction contributes around 6.0% producing H + $CO(OH)_2$ in the modified model.

With the temperature increasing, abstraction reactions become more dominant, accounting from 34.2% to 78.9%, especially by OH radicals. In contrast, unimolecular decomposition reactions come to be less effective. At 1000 K, they even have no impact on the oxidation of formic acid. The C–O bond in HOCO is easily cleaved at higher temperature, which leads to the formation of CO and OH radicals and the dominance of this reaction increases with the branching ratio rising from 9.9 to 90.5%. Besides, OH addition reaction comes to be more important ac-

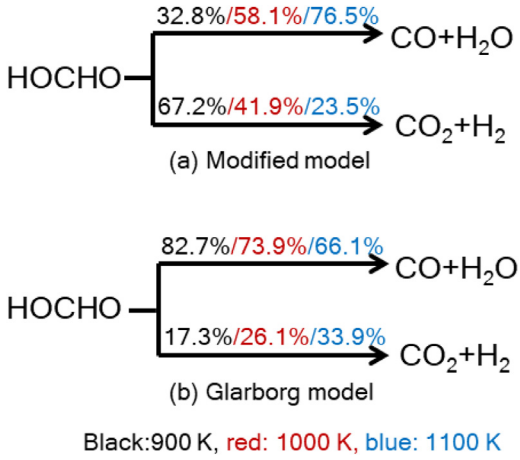

Fig. 14. Flux analysis for the pyrolysis of HOCHO at 900 K, 1000 K and 1100 K and $\phi = 1.0$ using Modified model and Glarborg model.

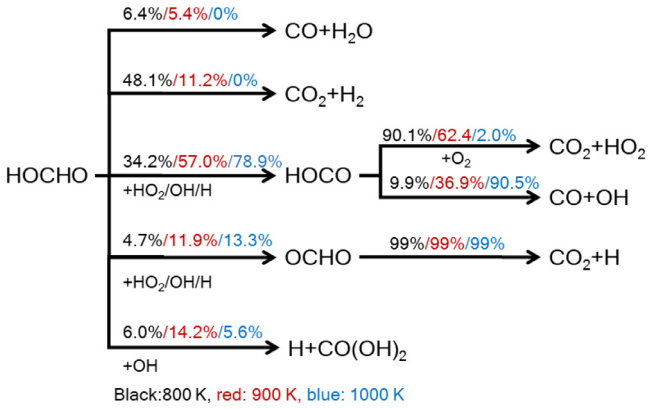

Fig. 15. Flux analysis for the oxidation of HOCHO at 800 K, 900 K and 1000 K and $\phi = 1.0$ by Modified model.

counting for 14.2% at 900 K but drops at 1000 K which means this reaction class can not be neglected at low temperature range.

5.3. Sensitivity analyses

Sensitivity analysis for formic acid at $\phi = 1.0$, 900 K was conducted and shown in Fig. 16. It indicates that H abstraction reaction by HO_2 (HOCHO + HO_2<=>HOCO + H_2O_2) is the most promoting reactivity reaction in this system as it effectively convert the less reactive HO_2 to H_2O_2 which further decomposes to two OH radicals through the following sequence: H_2O_2<=>OH + OH. Thus, decomposition of H_2O_2 also promotes the oxidation of HOCHO significantly. HOCO and OCHO are majorly produced via H abstraction reaction. The decomposition of these radicals plays strong positive roles in the oxidation process to produce OH and H radicals. Because of this, there is an interesting phenomenon that abstraction reactions like HOCHO + OH<=>HOCO + H_2O, HOCHO + H<=>HOCO + H_2, HOCHO + OH<=>OCHO + H_2O promote but not inhibit reactivity, different from other fuels as the literatures shown [16]. In addition, the oxidation of formic acid is also sensitive to initial unimolecular decomposition reactions, HOCHO<=>CO + H_2O, HOCHO<=>CO_2 + H_2.

Reaction H_2O_2+H<=>H_2O+OH has the largest coefficient inhibiting the reactivity as it competes with this reaction H_2O_2<=>OH+OH. HO_2 related reactions have extensive effect on the reactivity because it is a significant radical with early and vast production. Reactions which consume active radicals and produce relatively stable species inhibit the overall reactivity, such as HO_2 + H<=>H_2 + O_2, HO_2 + OH<=>H_2O + O_2, and HO_2 + HO_2<=>H_2O_2 + O_2. In general, sensitivity analysis provides an overview of the formic acid reactions which control the reactivity. Low temperature oxidation of formic acid is mainly sensitive to fuel-related reactions as well as the following sequence of produced radicals, HOCO and HO_2.

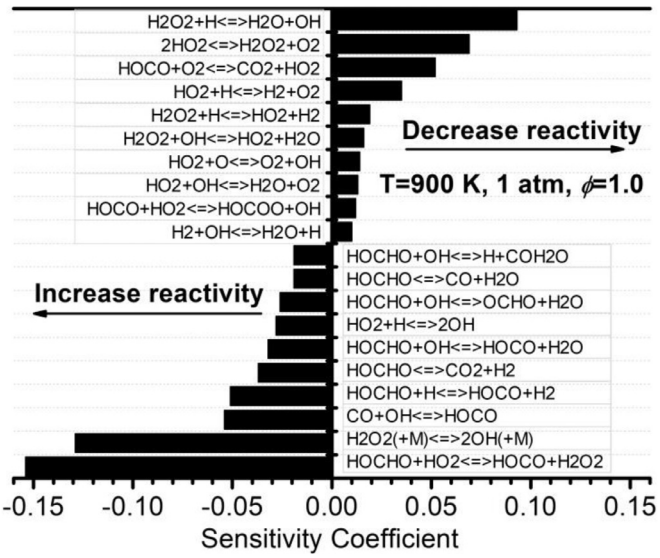

Fig. 16. Sensitivity analysis on low temperature oxidation of HOCHO.

5.4. Laminar flame speeds validations

In our previous work, the laminar flame speeds of formic acid were also measured at equivalence ratios of 0.4–1.6, initial temperatures of 423–453 K and atmospheric pressures. The simulated results using modified model still match well with experimental data [14] presented in Fig. 17. Besides, the flame speed reported by Sarathy et al. [34] was used to validate the model as shown in Fig. 18. The modified model is able to provide reasonable prediction on measured laminar flame speeds. Figure S5 in Supplemental data 1 also compares the present model against measurements by de Wilde and van Tiggelen [13] obtained in High oxygen content mixed with N_2. However, modified model shows big discrepancy with the experimental data under high N_2 dilutions. Similar levels of agreement were observed by Glarborg model as dashed lines shown and Sarathy et al. [34].

6. Conclusions

In this work, experimental and kinetic study on low temperature oxidation and pyrolysis of formic acid in a jet-stirred reactor was performed. A detailed chemical kinetic model of formic acid was also developed based on the Glarborg model using the combination method of ab initio calculations and estimates according to the mole profiles of stable species. Good prediction on experimental data of speciation results in low temperature oxidation and pyrolysis in JSR as well as laminar flame speeds can be achieved using the Modified model. Meanwhile, pathway and sensitivity analysis were conducted to provide an overview on the low to intermediate temperature oxidation process.

At 800 K, the major pathway is unimolecular decomposition reactions while H abstraction reactions become much more important with temperature increasing. The largely produced HOCO radicals tend to be consumed through O_2 addition reaction and thermal dissociation at low and high temperature, respectively. OH

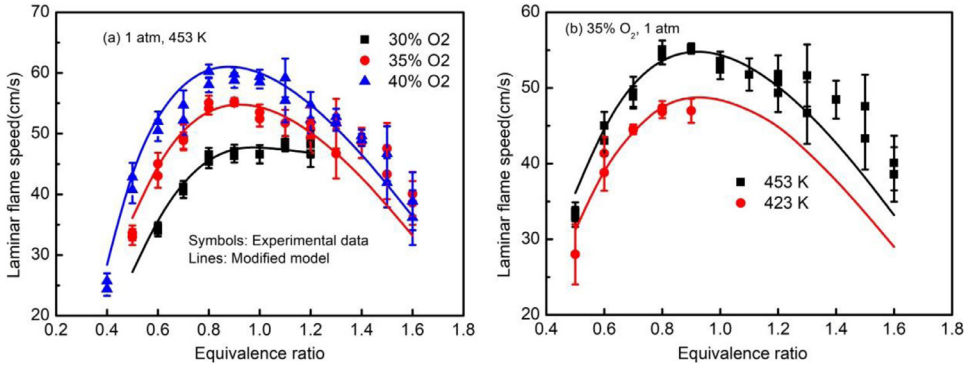

Fig. 17. Experimental and simulated laminar flame speeds of HOCHO using Modified model.

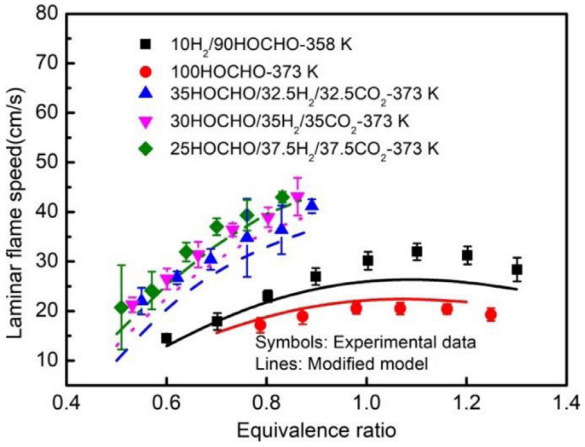

Fig. 18. Comparison of the present model with data for $HOCHO/O_2/N_2$ from Sarathy et al. [34].

addition reaction is important at the current temperature range. For pyrolysis, the thermal dissociation of HOCHO is unusual that its two product channels yield only stable species rather than radicals. As to sensitivity analysis, the oxidation of formic acid is very sensitive to H abstraction reactions. The largest promoting one is found for the reaction of HOCHO with HO_2 to form HOCO and H_2O_2 with the latter further decomposing to two OH radicals quickly. While the largest inhibited one is H_2O_2 related reaction which competes with the decomposition of H_2O_2 and serve to slow down the overall reactivity.

Declaration of Competing Interest

The authors declare that they have no known competing financial interests or personal relationships that could have appeared to influence the work reported in this paper.

Acknowledgments

This study is supported by the Natural Science Foundation of Shaanxi Province for Distinguished Young Scholars (2020JC-04), the National Natural Science Foundation of China (51888103, 51876163, 91641124) and Young Talent Support Plan of Shaanxi Province. The supports from Science and Technology on Combustion, Internal Flow and Thermal-structure Laboratory (6142701190401) and the Fundamental Research Funds for the Central Universities and are also appreciated.

Supplementary materials

Supplementary material associated with this article can be found, in the online version, at doi:10.1016/j.combustflame.2020.10.005.

References

[1] J.E. Lawrence, P. Koutrakis, Measurement of atmospheric formic and acetic acids: methods evaluation and results from field studies, Environ. Sci. Technol. 28 (1994) 957–964.
[2] A. Chebbi, P. Carlier, Carboxylic acids in the troposphere, occurrence, sources, and sinks: a review, Atmos. Environ. 30 (1996) 4240–4249.
[3] A. Oasrnaa, Y. Solantausta, V. Arpiainen, E. Kuoppala, K. Sipilae, Fast pyrolysis bio-oils from wood and agricultural residues, Energy Fuel 24 (2010) 1380–1388.
[4] J. Eppinger, K.W. Huang, Formic acid as a hydrogen energy carrier, ACS Energy Lett. 2 (2016) 188–195.
[5] Chang J.G., H.T. Chen, S. Xu, M. Lin, Computational study on the kinetics and mechanisms for the unimolecular decomposition of formic and oxalic acids, J. Phys. Chem. A 111 (2007) 6789–6797.
[6] M.J. Anglada, Complex mechanism of the gas phase reaction between formic acid and hydroxyl radical. Proton coupled electron transfer versus radical hydrogen abstraction mechanisms., J. Am. Chem. Soc. 126 (2004) 9809–9820.
[7] H.G. Yu, G. Poggi, J.S. Francisco, J.T. Muckerman, Energetics and molecular dynamics of the reaction of HOCO with HO(2) radicals, J. Chem. Phys. A 129 (2008) 214307.
[8] H.G. Yu, J.T. Muckerman, Quantum molecular dynamics study of the reaction of O_2 with HOCO†, J. Phys. Chem. A 110 (2006) 5312–5316.
[9] P.G. Blake, H.H. Davies, G.E. Jackson, Dehydration mechanisms in the thermal decomposition of gaseous formic acid, J. Chem. Soc. B 10 (1971) 1923–1925.
[10] D. Golden, G. Smith, A.B. McEwen, C.L. Yu, B. Eiteneer, M. Frenklach, G.L. Vaghjiani, A.R. Ravishankara, F.P. Tully, OH(OD) + CO: measurements and an optimized RRKM Fit, J. Chem. Phys. A 102 (1998) 8598–8606.
[11] A.G. Gaydon, H.G. Wolfhard, Spectroscopic studies of low-pressure flames, Combust. Flame Explos. 3 (1949) 504–518.
[12] P. Marshall, P. Glarborg, Ab initio and kinetic modeling studies of formic acid oxidation, Proc. Combust. Inst. 35 (2015) 153–160.
[13] E. de Wilde, A. van Tiggelen, Burning velocities in mixtures of methyl alcohol, formaldehyde or formic acid with oxygen, Bull. Soc. Chim. Belg. 77 (1968) 67–75.
[14] G. Yin, Q. Gao, E. Hu, J. Xu, Z. Huang, Experimental and kinetic study on laminar flame speeds of formic acid, Combust. Flame 220 (2020) 73–81.
[15] C. Zhou, Y. Li, U. Burke, C. Banyon, K.P. Somers, S. Ding, et al., An experimental and chemical kinetic modeling study of 1,3-butadiene combustion: ignition delay time and laminar flame speed measurements, Combust. Flame 197 (2018) 423–438.
[16] G. Yin, Z. Gao, E. Hu, Z. Xu, Z. Huang, Comprehensive experimental and kinetic study of 2,4,4-trimethyl-1-pentene oxidation, Combust. Flame 208 (2019) 246–261.
[17] Z. Gao, E. Hu, Z. Xu, G. Yin, Z. Huang, Low to intermediate temperature oxidation studies of dimethoxymethane/n-heptane blends in a jet-stirred reactor, Combust. Flame 207 (2019) 20–35.
[18] D.G. Truhlar, A.D. Isaacson, B.C. Garrett, Theory of chemical reaction dynamics, Nato Sci. 170 (1986) 65–137.
[19] I.M. Alecu, J. Zheng, Y. Zhao, D.G. Truhlar, Computational thermochemistry: scale factor databases and scale factors for vibrational frequencies obtained from electronic model chemistries, J. Chem. Theory Comput. 6 (2010) 2872–2887.
[20] G. Knizia, H.J. Werner, Explicitly correlated RMP2 for high-spin open-shell reference states, J. Chem. Phys. 128 (2008) pp. 154103-154100.

[21] M.P. Andersson K, B.O. Roos, Second-order perturbation theory with a complete active space self-consistent field reference function, J. Chem. Phys. 96 (1992) 1218–1226.
[22] D. Feller, D.A. Dixon, Extended benchmark studies of coupled cluster theory through triple excitations, J. Chem. Phys. 115 (2001) 3484–3496.
[23] Y. Georgievskii, S.J. Klippenstein, Variable reaction coordinate transition state theory: analytic results and application to the C2H3+H→C2H4 reaction, J. Chem. Phys. 118 (2003) 5442–5455.
[24] Y. Georgievskii, J.A. Miller, M.P. Burke, S.J. Klippenstein, Reformulation and solution of the master equation for multiple-well chemical reactions, J. Phys. Chem. A 117 (2013) 12146–12154.
[25] S.J. Klippenstein, Variational optimizations in the Rice–Ramsperger–Kassel–Marcus theory calculations for unimolecular dissociations with no reverse barrier, J. Chem. Phys. 96 (1992) 367–371.
[26] M.J. Frisch, G.W. Trucks, H.B. Schlegel, G.E. Scuseria, M.A. Robb, J.R. Cheeseman, et al. Gaussian 09, revision D.02. (2009).
[27] Y. Georgievskii, S.J. Klippenstein, Transition state theory for multichannel addition reactions: multifaceted dividing surfaces, J. Phys. Chem. A 118 (2003) 5442–5455.
[28] H.J. Werner, P.J. Knowles, F.R. Manby, M. Schütz, P. Celani, G. Knizia, et al. MOLPRO, version 2018.1, a package of ab initio programs. (2018).
[29] T.J. Lee, P.R. Taylor, A diagnostic for determining the quality of single-reference electron correlation methods, Int. J. Quantum Chem. 36 (1989) 199–207.
[30] C.W. Zhou, J.M. Simmie, K.P. Somers, C.F. Goldsmith, H.J. Curran, Chemical kinetics of hydrogen atom abstraction from allylic sites by $^3O_2$; implications for combustion modeling and simulation, J. Phys. Chem. A 121 (2017) 1890–1899.
[31] C.F. Goldsmith, S.J. Klippenstein, W.H. Green, Theoretical rate coefficients for allyl+HO_2 and allyloxy decomposition, Proc. Combust. Inst. 33 (2011) 273–282.
[32] S.J. Klippenstein, L.B. Harding, M.J. Davis, A.S. Tomlin, R.T. Skodje, Uncertainty driven theoretical kinetics studies for CH_3OH ignition: HO_2+CH_3OH and O_2+CH_3OH, Proc. Combust. Inst. 33 (2011) 351–357.
[33] M. Klatt, M. Rhrig, H.G. Wagner, About the radical formation in the pyrolysis of formic acid at high temperatures, Z. Naturforschung A 47 (1992) 1138–1140.
[34] S.M. Sarathy, P. Brequigny, A. Katoch, A.M. Elbaz, W.L. Roberts, R.W. Dibble, et al., Laminar burning velocities and kinetic modeling of a renewable e–fuel: formic acid and its mixtures with H_2 and CO_2, Energy Fuel 34 (2020) 7564–7572.